2014

Prediction of Evaporator Frosting in Household Refrigerators Subjected to Periodic Door Opening

Bruno N. Borges
Federal University of Santa Catarina, brunoborges@polo.ufsc.br

Cláudio Melo
Federal University of Santa Catarina, melo@polo.ufsc.br

Christian J. L. Hermes
Federal University of Paraná, chermes@ufpr.br

Prediction of Evaporator Frosting in Household Refrigerators Subjected to Periodic Door Opening

Bruno N. BORGES [1], Cláudio MELO [1], Christian J. L. HERMES [2,*]

[1] POLO - Research Laboratories for Emerging Technologies in Cooling and Thermophysics
Department of Mechanical Engineering, Federal University of Santa Catarina
88040-900, Florianópolis, SC, Brazil, +55 48 3234 5691

[2] Laboratory of Thermodynamics and Thermophysics,
Department of Mechanical Engineering, Federal University of Paraná
81531-990, Curitiba, PR, Brazil, +55 41 3361 3239

[*] Corresponding author: chermes@ufpr.br

ABSTRACT

This paper describes a quasi-steady-state simulation model for predicting the transient behavior of a household refrigerator subjected to periodic door opening. A semi-empirical steady-state sub-model was developed for the refrigeration loop, and a transient sub-model was devised to predict the energy and mass transfer into and within the refrigerated compartments as well as the evaporator frosting. The key empirical heat and mass transfer parameters required by the model were derived from a set of experiments carried out in a climate-controlled chamber. In general, it was found that the model predictions followed closely the experimental trends for the power consumption (deviations within ±10%) and for the compartment temperatures (deviations within ±2 K).

1. INTRODUCTION

Modern refrigerator design is aimed at energy savings and also at product robustness in relation to evaporator frosting. In this regard, standardized tests as well as tests under real usage conditions, that is, with doors opened regularly allowing moisture to enter the refrigerated compartment and frost to accumulate on the evaporator coil (Piucco et al., 2011), are procedures commonly carried out by most manufacturers.

Nevertheless, since the experimental procedures are costly and time consuming (Hermes *et al*., 2013), simulation models are constantly being devised to improve the product development process (Hermes and Melo, 2008; Gonçalves *et al*., 2009; Hermes *et al*., 2009a; Negrão and Hermes, 2011; Mitishita *et al.,* 2013). However, to the best of the authors' knowledge, none of the models available in the literature are able to predict the refrigerator performance under periodic door opening, which is the main focus of this study.

The current model follows a quasi-steady-state approach (Borges *et al*., 2011), with a steady-state sub-model for the refrigeration loop and a transient sub-model for the energy and moisture transfer into and within the refrigerated compartments. An additional frost growth and densification sub-model was also developed to predict the frost accumulation on the evaporator coil over time. The key heat and mass transfer empirical parameters needed to complete the model were derived from experiments carried out in a climate-controlled chamber.

2. SIMULATION MODEL

2.1 Refrigeration Loop

A 433-liter top-mount refrigerator, running with R-134a and comprised of a 6.76-cm^3 hermetic reciprocating compressor, natural draft wire-on-tube condenser, tube-fin evaporator and capillary tube-suction line heat exchanger, also known as internal heat exchanger (Figure 1), was used in this study. Sub-models for each of the system components were developed following closely the work of Borges *et al*. (2011).

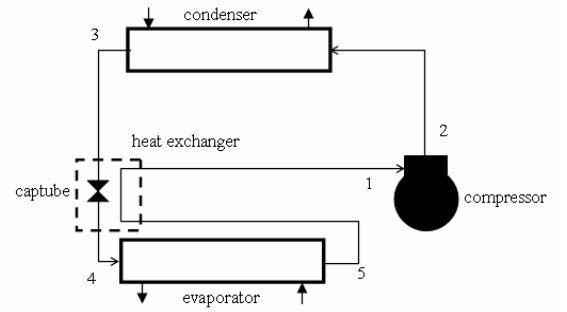

Figure 1: Schematic representation of the refrigeration loop

Compressor

The compressor sub-model uses the volumetric (η_v) and overall (η_g) efficiencies to calculate the compression power and the refrigerant mass flow rate for a given operating condition. The compressor shell thermal conductance (UA_k) is also required for the heat transfer calculation. The refrigerant specific enthalpy at the compressor outlet is thus obtained from the following energy balance:

$$h_2 = h_1 + \left(h_{2,s} - h_1\right)/\eta_g - UA_k\left(T_2 - T_a\right)/m_r \tag{1}$$

where $m_r=\eta_v NS/v_1$ is the mass flow rate displaced by the compressor, N and S are the compressor speed and the swept volume, respectively, and $W=(h_{2,s}-h_1)/\eta_g$ is the compression power. The compression efficiencies were fitted to the experimental data as linear functions of the pressure ratio and the UA_k coefficient was expressed as a linear fit to the surrounding air temperature data. Further details on the compressor model can be found in Borges (2013).

Capillary tube suction line heat exchanger

The internal heat exchanger was modeled according to the semi-empirical approach introduced by Hermes *et al.* (2010), who considered the refrigerant flow and the heat transfer as independent phenomena, and derived explicit algebraic expressions for the refrigerant mass flow rate and the heat exchanger effectiveness (ε_x). The specific enthalpy at the evaporator inlet and the temperature at the compressor inlet are thus expressed as:

$$h_4 = h_3 - \varepsilon_x c_{p,l}\left(T_3 - T_5\right) \tag{2}$$

$$T_1 = T_5 + \varepsilon_x\left(T_3 - T_5\right) \tag{3}$$

Condenser

The natural draft wire-and-tube condenser was divided into three parts, namely superheating, saturation and subcooling (Gonçalves et al., 2009). The specific refrigerant enthalpy at the condenser outlet is expressed as:

$$h_3 = h_2 - UA_c\left(T_c - T_a\right)/m_r \tag{4}$$

As the heat transfer is governed by free convection and radiation on the air-side, the thermal conductance was approximated as $UA_c \approx \alpha_c A_c$. The combined heat transfer coefficient was calculated from the correlation proposed by Melo and Hermes (2009). The condensing pressure was calculated implicitly ensuring that the compressor mass flow rate equals the capillary tube mass flow rate.

Evaporator

The evaporator sub-model was divided into two domains, namely the refrigerant flow and the air-side heat and mass transfer. The specific refrigerant enthalpy at the evaporator outlet can be expressed as:

$$h_5 = h_4 + \left(Q_{sen} + Q_{lat}\right)/m_r \tag{5}$$

where $h_5=h(p_e,T_5)$ and $T_5=T_e+\Delta T_{sup}$.

The evaporator superheating, ΔT_{sup}, varies with time due to the periodic door openings. To address this issue a moving-boundary approach, as introduced by Wedekind and Stoecker (1968), was adopted:

$$\zeta = \zeta_{ss} - \left(\zeta_{ss} - \zeta^{\circ}\right)\exp\left(-\tau\Delta t\right) \tag{6}$$

where $\zeta_{ss}=(1-x_4)m_r^{o}h_{lv}/q'$ is the two-phase boundary position in the steady-state regime, m_r^{o} (=3.8 kg/h) is the initial mass flow rate under steady-state conditions, $\tau=(1-\gamma)\rho_l h_{lv}A_c/q'$ is a time constant, $q'=m_r(h_v-h_4)/\zeta$ is the heat transfer rate per unit length in the two-phase region, and γ is the mean void fraction of the two-phase region, calculated as suggested by Cioncolini and Thome (2012).

2.2 Evaporator Frosting

The evaporator sub-model calculates the cooling capacity from the following heat and mass balances on the air-side:

$$Q_{sen} = m_a c_{p,a}\left(T_f - T_i\right)\left[1-\exp\left(-\alpha_e A_e / m_a c_{p,a}\right)\right] \tag{7}$$

$$Q_{lat} = m_a h_{sv}\left(w_f - w_i\right)\left[1-\exp\left(-\alpha_e A_e / m_a c_{p,a} Le^{2/3}\right)\right] \tag{8}$$

where $Q_e=Q_{sen}+Q_{lat}$, T_f is the frost surface temperature, $w_f=w_{sat}(T_f)$ is the humidity ratio at the frost surface, Le is the Lewis number and α_e is the air-side heat transfer coefficient calculated as suggested by Barbosa *et al*. (2009). The frost formation model was based on the work of Hermes *et al.* (2009b). This model was originally developed for horizontal flat surfaces and later adapted by Knabben *et al.* (2011) for finned-tube heat exchangers (Figure 2).

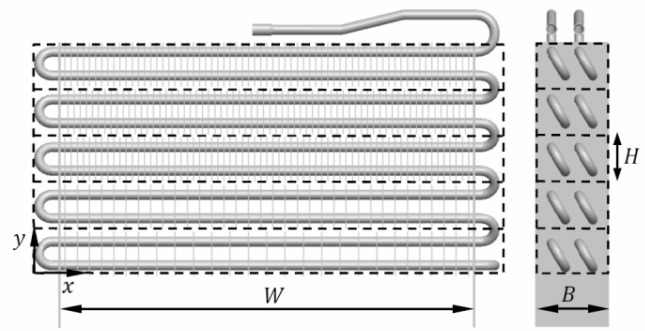

Figure 2: Schematic representation of the so-called "no-frost" evaporator coil

According to Hermes et al. (2009b), the frost surface temperature is calculated from:

$$T_f = T_e + Q_e\delta / k_f A_s + \left(w_{sat,e} h_{sv}\rho_a D_f / k_f\right)\left(1-\cosh Ha\right) \tag{9}$$

where Ha is the Hatta number and k_f and D_f are the effective thermal conductivity and vapor diffusivity of the frost layer, respectively. In addition, the growth rate of the frost layer of thickness δ_f is calculated from (Hermes et al., 2009b):

$$\frac{d\delta}{dt} = \frac{2k_f}{b\rho_f \delta h_{sv}}\left[\sqrt{\left(1+\frac{b\delta Q_{sen}}{k_f A_e}\right)^2 + \frac{4b\delta h_{sv}}{k_f}G_f} - \left(1+\frac{b\delta Q_{sen}}{k_f A_e}\right)\right] \tag{10}$$

where G_f is the total mass flux of the vapor transferred to the frosted medium, and b is an empirical parameter that comes from the frost density correlation in the form $\rho_f=a\cdot\exp(b\cdot T_s)$ (Hayashi *et al.*, 1977). The accumulated frost mass and the frost growth are calculated, respectively, from $m_f=m_f^{o}+G_f A_e\Delta t$ and $\delta_f=\delta_f^{o}+(d\delta_f/dt)\Delta t$. In addition, the frost density is obtained from $\rho_f(t>0)=m_f^{o}/A_e\delta_f^{o}$, where the superscripted $(\,)^{o}$ represents the values at the previous time-step.

2.3 Refrigerated Compartments

The air temperature and humidity of the fresh-food and freezer compartments are expressed, respectively, as (Borges *et al.*, 2011):

$$T_* = T_{ss,*} - \left(T_{ss,*} - T_*^\circ\right)\exp\left(-A_*\Delta t / C_*\right) \tag{11}$$

$$w_* = w_{ss,*} - \left(w_{ss,*} - w_*^\circ\right)\exp\left(-B_*\Delta t / \rho_*\phi_*\right) \tag{12}$$

where T_*° and w_*° are the air temperature and humidity ratio of the compartment at the beginning of the time-step. $A_*=UA_*+UA_m+m_{d,*}c_{p,a}+m_*c_{p,a}$ and $B_*=m_{d,*}+m_*$. The asterisk ( )$_*$ indicates either the freezer (fz) or the fresh-food (ff) compartment. The thermal conductance of each compartment, UA_*, and of the mullion, UA_m, and the equivalent thermal capacity and mass of each compartment, C_* and ϕ_*, respectively, were all obtained from experimental data. In addition, the terms $T_{ss,*}$ and $w_{ss,*}$ are related to the steady-state condition.

The air flow rate entering the cabinet during a door opening event is calculated as described in the literature (Wang, 1990) and shown in Figure 3 as follows:

$$m_{d,*} = \frac{2}{3}K_*\rho_* W_{d,*} H_{d,*}\sqrt{\frac{2gH_{d,*}\left(1-\rho_a/\rho_*\right)}{\left(1+\left(\rho_*/\rho_a\right)^{1/3}\right)^3}} \tag{13}$$

where K_* is an empirical discharge coefficient determined from experimental data (Borges, 2013). The state of the air returning to the evaporator was calculated from $T_r=rT_{fz}+(1-r)T_{ff}$, where r is the freezer air flow ratio (Borges *et al.*, 2011).

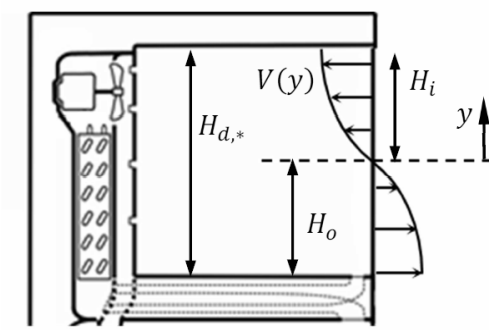

Figure 3: Schematic representation of the air flow during a door opening event

The air-side hydrodynamics was modeled according to the methodology outlined in Hermes *et al.* (2009a). The overall pressure drop was thus correlated to the air flow rate through the following expression:

$$\Delta p_t = c\rho_a V^2 + \Delta p_e \tag{14}$$

where c is an empirical coefficient obtained from experimental data and Δp_e is the pressure drop in the frosted evaporator. This parameter was calculated as suggested by Kays and London (1984), using the friction factor proposed by Barbosa *et al.* (2009) for "no-frost" evaporators. The characteristic curve for the fan was fitted to a third-order polynomial using experimental data obtained in a wind-tunnel facility (Borges, 2013).

2.4 Solution Algorithm

The model was coded in EES (Klein, 2011). The solution algorithm, illustrated in Figure 4, is based on a sequential solution for the models for the refrigerated compartments and the refrigeration loop, whose sub-models are in turn solved simultaneously by the Newton-Raphson technique. The evaporator frosting and dry-out sub-models are solved implicitly in the inner loop, whereas the models for the refrigerated compartments are solved explicitly in an outer loop, as depicted in Figure 4. The on-off cycles were implemented by means of an IF-THEN-ELSE loop that emulates a thermostat. The door opening patterns are included in the model in an outer loop, as shown in Figure 4.

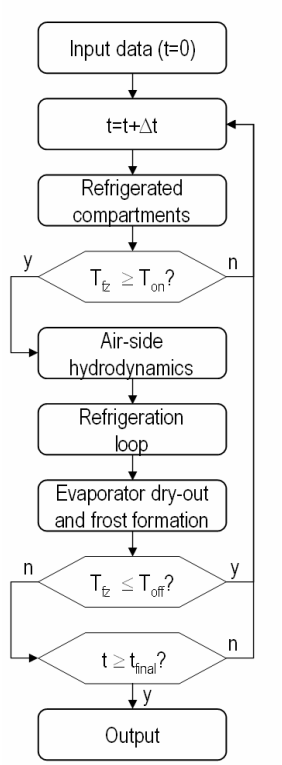

Figure 4: Information flow diagram of the simulation model

3. EXPERIMENTAL WORK

The refrigerator was carefully instrumented as illustrated in Figure 5. The experimental plan, summarized in Table 1, was designed to provide all of the empirical information required for the sake of model closing. The doors were opened and closed using a purpose-built door-opening device attached to both the freezer and fresh-food doors (Piucco *et al*., 2011), so that they could be operated independently. The time between door opening events and the length of time of the event are both easily programmed. Patterns comprised of 3 cycles of door opening events, each cycle lasting 1 hour and applied in sequence, were adopted, with a 4-hour interval between cycles. After this period, the system was kept running for 8 hours with the doors closed. The pattern was repeated every 24 hours. In a door opening cycle, the freezer door was opened every 12 min for 10 seconds over a period of 1 hour, totalizing 5 opening events per hour. On the other hand, the fresh-food door was opened every 2.5 min for 30 seconds, totalizing 20 opening events per hour.

Table 1: Summary of experimental tests

Experiment	Test facility	Ambient conditions	Empirical parameter
Fan characteristics	wind-tunnel	21°C, 50% RH	third-order polynomial
Cabinet hydrodynamics	wind-tunnel	21°C, 50% RH	c
Refrigeration loop	chamber	6 runs, doors closed, 25<T<38°C, 8<w<32g/kg	r, η_v, η_g, UA_k, UA_*, UA_m, C_*
Door opening tests	chamber	3 runs, door opening, 25<T<38°C, 12<w<21g/kg	K_*, ϕ_*, ρ_f^o, m_r^o, b

4. RESULTS

The model predictions were compared with the corresponding experimental data for ambient conditions of 32°C and 70% RH. The simulations were initiated at the compressor start up immediately after a defrost cycle and lasted until the next defrost cycle began. Figure 6 shows the predicted and experimental results for the refrigerated compartment temperatures for the whole period. Two door opening cycles can be clearly seen, the first from 30 to 120 min and the second from 345 to 405 min. It should be noted that the model follows closely the experimental trends, with an average deviation of around ±2°C, the maximum discrepancies occurring during door opening.

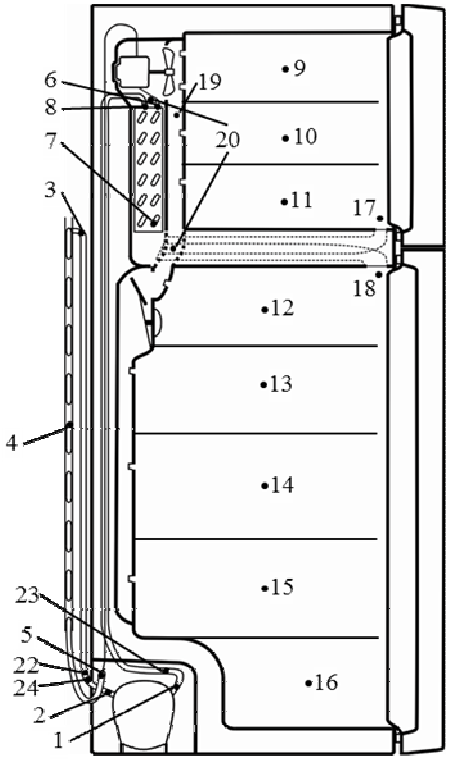

	Measurement	Instrument
1	Compressor discharge temperature.	T-type TC
2	Compressor suction temperature	T-type TC
3	Condenser inlet temperature	T-type TC
4	Condenser mid temperature	T-type TC
5	Condenser outlet temperature	T-type TC
6	Evaporator inlet temperature	T-type TC
7	Evaporator mid temperature	T-type TC
8	Evaporator outlet temperature	T-type TC
9-11	Freezer compartment temperatures	T-type TC
12-16	Fresh-food compartment temperatures	T-type TC
17	Freezer humidity	Capacitive sensor
18	Fresh-food comp. humidity	Capacitive sensor
19	Evaporator outlet humidity	Capacitive sensor
20	Air pressure-drop across evaporator	Strain-gauge
21	Defrost water mass	Load-cell
22	Refrigerant mass flow rate	Coriolis-type
23	Evaporating pressure	Strain-gauge
24	Condensing pressure	Strain-gauge

Figure 5: Summary of the instrumentation

Figure 7 compares the time-evolution predictions of the working pressures with the experimental data. It can be observed that the model predictions for the evaporating pressure are within a ±5% error band, while the condensing pressure is under predicted with an offset of approximately 0.5 bar during the whole period, but with deviations within a ±10% error band. Consequently, the power consumption is also reasonably well predicted by the model, with deviations not exceeding ±5%, as shown in Figure 8.

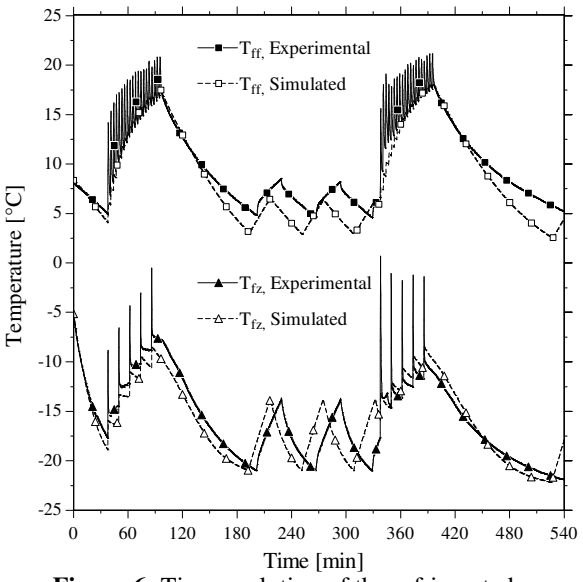

Figure 6: Time evolution of the refrigerated compartment temperatures

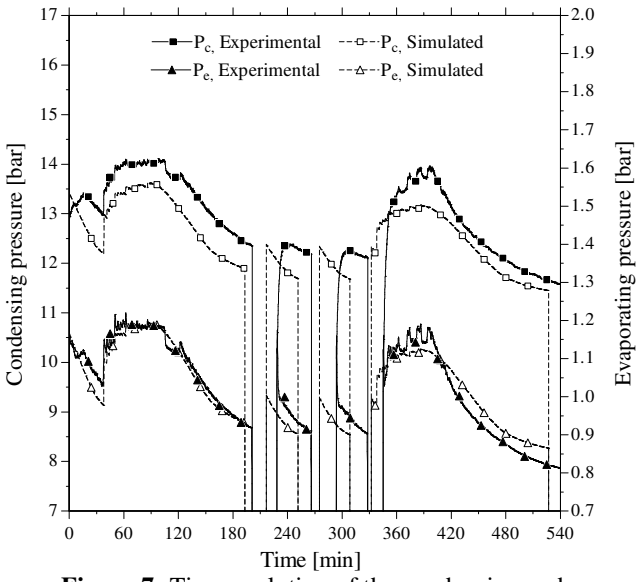

Figure 7: Time evolution of the condensing and evaporating pressures

Figure 9 shows the time-evolution of the evaporator superheating. Five peaks can be observed during the test period, which appear when both doors are opened concurrently, thus increasing the thermal loads and pushing the dry-out position downstream of the evaporator. Small variations in the evaporator superheating occur when only the door of the fresh-food compartment is opened. It can also be noted that model predictions follow the experimental trends satisfactorily, although errors of up to 2 K are observed in the peaks.

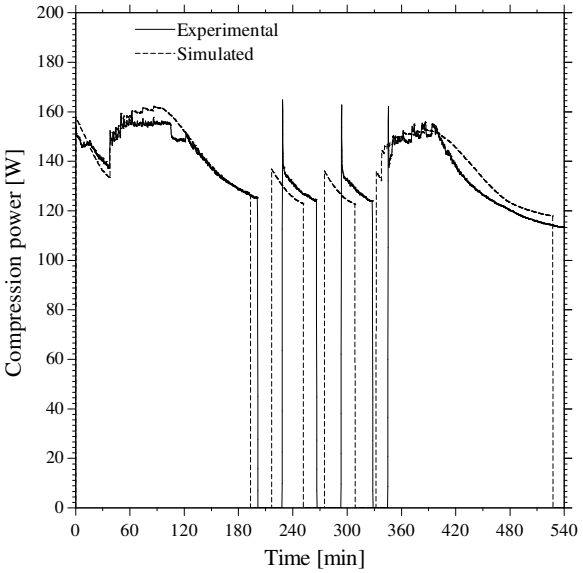

Figure 8: Time evolution of the compression power

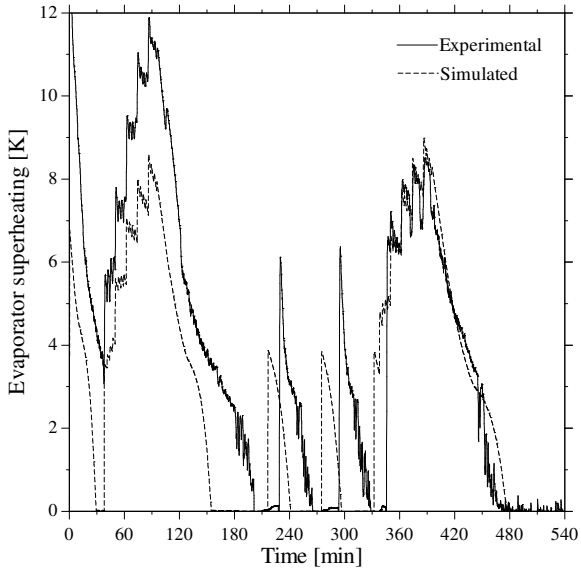

Figure 9: Time evolution of the evaporator superheating

Figure 10 shows the time-evolution of the air-side pressure drop due to evaporator frosting and Fig. 11 explores the air-side prediction capabilities of the model. For a clean evaporator coil, a 5 Pa pressure drop is observed in Fig. 10, increasing steadily to 15 Pa during the first cycle of door opening events. This value does not change during the period when the doors are kept closed (from ~180 to ~360 min), since there is no moisture infiltration and, therefore, no frost growth. During the second cycle of door openings the evaporator air-side pressure drop increases to around 25 Pa. During the whole period the model predicted satisfactorily the experimental trends, although absolute errors of up to 5 Pa can be observed.

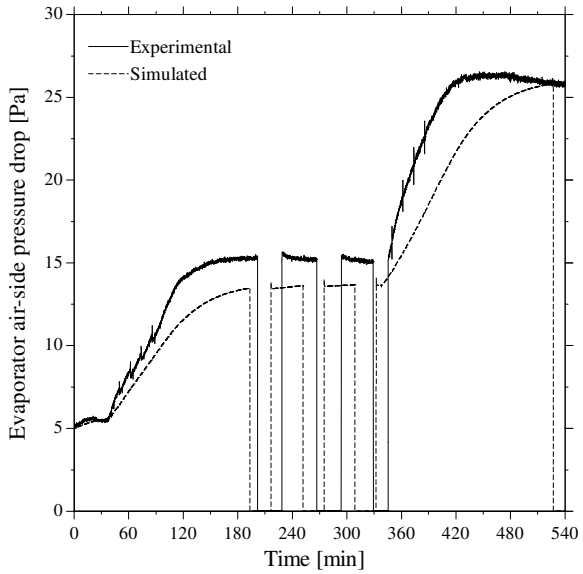

Figure 10: Time evolution of the evaporator air-side pressure drop

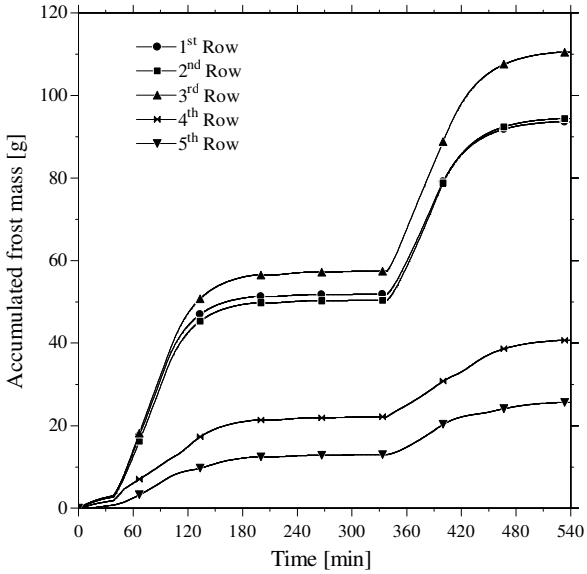

Figure 11: Time evolution of the accumulated frost mass along each evaporator row

Figure 11 shows the calculated frost mass for each of the five evaporator rows. The rows are numbered from bottom to top, according to the air flow direction, as illustrated in Figure 2, and comprised 27 (1st), 34 (2nd), 67 (3rd), 66 (4th), and 67 (5th) fins. It can be noted that the frost is mostly accumulated along the first three rows, which is due to the higher humidity gradient at the evaporator inlet. It can also be noted that there is more frost accumulated along the 3rd row than along the 1st row, which is due to the higher heat transfer (finned) area of the former.

5. CONCLUDING REMARKS

A quasi-steady-state semi-empirical mathematical model was developed to predict the transient behavior of the key operating parameters of a frost-free refrigerator, that is, the working pressures, compression power, compartment temperatures and accumulated frost mass on the evaporator coil. The model predictions were compared with a set of in-house experimental data collected in a climate-controlled chamber. The door opening were carried out by a purpose-built apparatus according to a predefined pattern. It was found that the model predictions followed closely the experimental trends, with deviations for the working pressures and power consumption not exceeding the 10% thresholds and predictions for the compartment air temperatures being within ±2ºC error bands. The model was also used to predict the frost distribution over the evaporator coil and it was observed that the frost accumulates mostly in the first three rows, the third row being crucial in terms of frost clogging because of the higher number of fins and thus lower free flow passage of air.

NOMENCLATURE

Roman

A, heat transfer area, m^2
C, thermal capacity, J/K
c_p, specific heat at constant pressure, J/kgK
D, vapor diffusivity in air, m^2/s
G, mass flux, kg/m^2s
h, specific enthalpy, J/kgK
Ha, Hatta number, dimensionless
h_{lv}, latent heat of evaporation, J/kgK
h_{sv}, latent heat of sublimation, J/kgK
k, thermal conductivity, W/mK
Le, Lewis number, dimensionless
m, mass flow rate, kg/s
N, compressor speed, Hz
p, pressure, Pa
Q, heat transfer rate, W
r, air flow ratio
S, compressor swept volume, m^3
T, temperature, K
UA, thermal conductance, W
V, volumetric air flow rate, m^3/s
v, specific volume, m^3/kg
W, compression power, W
W, width, m
w, humidity ratio, kg_v/kg_a

Greek

α, heat transfer coefficient, W/m^2K
δ, frost thickness, m
ε_x, heat exchanger effectiveness, dimensionless
ϕ, correction factor, kg_v
Δp, pressure drop, Pa
Δt, time-step, s
η_g, global compression efficiency, dimensionless
η_v, volumetric compression efficiency, dimensionless
ρ, density, m
ζ, evaporator dry-out position, m

Subscripts

1, compressor inlet
2, condenser inlet
3, condenser outlet
4, evaporator inlet
5, evaporator outlet
a, ambient, air
c, condenser
d, door
e, evaporator
f, frost
ff, fresh-food
fz, freezer
i, inlet
k, compressor
l, saturated liquid
lat, latent thermal load
m, mullion
o, outlet
r, refrigerant
s, isentropic process
sat, saturation
sen, sensible thermal load
ss, steady-state
sup, superheating
v, saturated vapor

REFERENCES

Barbosa Jr., J. R. , Melo, C., Hermes, C. J. L. , Waltrich, P. J., 2009, A Study of the Air-Side Heat Transfer and Pressure Drop Characteristics of Tube-Fin No-Frost Evaporators, *Appl. Energy.*, vol. 86, no. 9: p. 1484-1491

Borges, B. N., 2013, *A Quasi-Steady Semi-Empirical Simulation Model for a Frost-Free Refrigerator under Periodic Door Opening Operation*, M. Eng. Thesis, Federal University of Santa Catarina, Florianópolis-SC, Brazil (in Portuguese)

Borges, B. N., Hermes, C. J. L., Goncalves, J. M., Melo, C., 2011, Transient Simulation of Household Refrigerators: A Semi-Empirical Quasi-Steady Approach, *Appl. Energy.*, vol. 88, no. 3: p. 748–754

Cioncolini, A., Thome, J. R., 2012, Void Fraction Prediction in Annular Two-Phase Flow, *Int. J. Multiphas. Flow* vol**.** 43, p. 72-84

Gonçalves, J. M. , Melo, C., Hermes, C. J. L., 2009, A Semi-Empirical Model for Steady-State Simulation of Household Refrigerators, *Appl. Therm. Eng.*, vol. 29,no. 8-9: p. 1622-1630

Hayashi, Y., Aoki, A., Adashi, S., Hori, K., 1977, Study of frost properties correlating with frost formation types, *ASME J. Heat Transfer,* vol. 99, p. 239-245

Hermes, C. J. L., Melo C., 2008, A First-Principles Simulation Model for the Start-up and Cycling Transients of Household Refrigerators, *Int. J. Refrig*., vol.31, no. 8: p. 1341-1357

Hermes, C. J. L., Melo, C., Knabben, F. T., 2010, Algebraic Solution of Capillary Tube Flows. Part II: Capillary Tube Suction Line Heat Exchangers, *Appl. Therm. Eng*., vol. 30, no. 5: p. 770-775

Hermes, C. J. L., Melo, C., Knabben, F. T., 2013, Alternative Test Method to Assess the Energy Performance of Frost-Free Refrigerating Appliances, *Appl. Therm. Eng*., vo. 50, no. 1: p. 1029-1034

Hermes, C. J. L., Melo, C., Knabben, F.T., Gonçalves, J. M., 2009a, Prediction of the Energy Consumption of Household Refrigerators and Freezers Via Steady-State Simulation, *Appl. Energy*., vol. 86,no. 7-8: p. 1311-1319

Hermes, C. J. L., Piucco, R. O., Melo, C., Barbosa Jr., J. R., 2009b, A study of Frost Growth and Densification on Flat Surfaces, *Exp. Therm. Fluid Sci*., vol. 33, no. 2: p. 371-379

Kays, W. M., London, A. L., 1984, *Compact Heat Exchangers*, 3rd ed., Krieger Publish Co., FL, USA.,

Klein, S. A., 2011, *Engineering Equation Solver*, v.8.954-3D, F-Chart Software, Madison-WI, USA

Knabben, F. T., Hermes, C. J. L., Melo, C., 2011, In-Situ Study of Frosting and Defrosting Processes in Tube-Fin Evaporators of Household Refrigerating Appliances, *Int. J. Refrig*., vol. 34, no. 8: p. 2031-2041

Melo, C., Hermes, C. J. L., 2009, A Heat Transfer Correlation for the Natural Draft Wire-and-Tube Condensers, *Int. J. Refrig*., vol.32,no. 3: p. 546-555

Mitishita, R. S., Barreira, E. M., Negrão, C. O. R. , Hermes, C. J. L., 2013, Thermoeconomic Design and Optimization of Frost-Free Refrigerators, *Appl. Therm. Eng*., vol. 50, no. 1: p. 1376-1385

Negrão, C. O. R., Hermes, C. J. L., 2011, Energy and Cost Savings in Household Refrigerating Appliances: A Simulation-Based Design Approach, *Appl. Energy*., vol. 88 no. 9: p. 3051–3060

Piucco, R. O., Hermes, C. J. L., Melo, C., 2011, In-Situ Evaluation of a Criterion to Predict Frost Formation on Liners of Refrigerated Cabinets, *Appl. Therm. Eng*., vol. 31,no. 14-15: p. 3084-3091

Wang, H., 1990, *Modelling of Refrigerating System Coupled with a Refrigerated Room*, PhD thesis, Delft University of Technology, The Netherlands

ACKNOWLEDGEMENTS

This study was carried out at the POLO facilities under National Grant No. 573581/2008-8 (National Institute of Science and Technology in Refrigeration and Thermophysics) funded by the Brazilian Government Agency CNPq. The authors are grateful to Mr. Rafael Gões for his valuable support in the experiments. Financial support from Whirpool Latin America S. A. is also duly acknowledged.